Report No. UCB/SEMM-2014/03	Structural Engineering Mechanics and Materials
	Development of Collapse Indicators for Risk Assessment of Older-Type Reinforced Concrete Buildings By Panagiotis H. Galanis, and Jack P. Moehle
April 2014	Department of Civil and Environmental Engineering University of California, Berkeley

DEVELOPMENT OF COLLAPSE INDICATORS FOR RISK ASSESSMENT OF OLDER-TYPE REINFORCED COCNRETE BUILDINGS

Panagiotis H. Galanis and Jack P. Moehle

ABSTRACT

This study examines the seismic collapse safety of older, non-ductile reinforced concrete building frames designed and constructed prior to 1980s. The study considered idealized buildings with heights ranging from four to twelve stories. Performance was gauged using non-linear dynamic analysis software considering nonlinearities associated with flexural yielding, shear failure, and axial failure. In addition to building height, the main variables were the relative strengths of columns and beams, and the relative shear and moment strengths in the columns. Incremental dynamic analysis was used to determine the probability of collapse for various combinations of the study variables. The results indicate that simple engineering indicators such as column-to-beam strength ratio and column flexural to shear strength ratio can be used to assess the collapse risk of older-type concrete buildings.

INTRODUCTION

The 1960s through 1970s was a period in which seismic design principles for reinforced concrete construction developed at a rapid rate. Buildings designed by these procedures are believed to have greater seismic resistance than those built using earlier procedures. Many buildings from around 1980 and earlier, however, in the United States and elsewhere, were constructed without consideration of these developments. Such buildings may have relatively low base-shear strength and may have details and proportions that result in low ductility/displacement capacity. Some of these buildings pose a high seismic risk to building occupants, and will be a major source of casualties in future earthquakes. An important goal is to be able to identify the highest risk buildings so that mitigation efforts can be directed to improve their safety.

One method for identifying high-risk buildings is to identify the codes to which they were designed. In the highly seismic western United States, modern requirements for design of ductile concrete buildings were introduced in building codes starting in 1976 (UBC, 1976). By 1980, these requirements were widely implemented. This benchmark year thus provides a date by which to classify older-type designs versus more modern-type designs. Unfortunately, in the counties of highest risk in California alone, approximately 17,000 such pre-1980 concrete buildings exist (EERI, 2011). In other parts of the United States and worldwide, the number of these buildings is very large. Retrofitting all these buildings clearly is impossible given economic, social, and political constraints. Alternative procedures are required.

In this paper we report results of a study to identify characteristics of older-type concrete buildings having highest risk of collapse. The study begins with three idealized building frames of different heights that were detailed to comply with current code provisions. These benchmark buildings were sequentially weakened by modifying transverse reinforcement and column-to-beam moment strength ratios. For each case, the collapse risk was evaluated to identify combinations that result in sudden changes in collapse risk. The intent is to develop a set of "collapse indicators" whose presence in a building can be used to indicate a higher propensity for collapse compared with the background population of older-type concrete buildings. The study is limited to regular, frames without torsion. The methodology, however, is applicable to other types of older concrete buildings.

IDEALIZED BUILDING FRAMES

The studied buildings have 4, 8, or 12 stories. The idealized buildings consist of twelve earthquake-resisting space frames, six in each direction, that were designed to resist both gravity and earthquake forces. Gravity loads comprise dead load (including the self-weight of the structural components) of 150 psf, cladding load of 15 psf, and service live load of 60 psf. The design seismic loading was idealized as an inverted triangular loading with total base-shear equal to $0.1W$, where W is the total building weight. Each frame was assumed to resist one-sixth of the total lateral force in each direction. The design base-shear $0.1W$ was expected to result in actual base-shear strength

around 0.15W to 0.20W, which is typical for base-shear strength for this type of building. Results of collapse analyses can be normalized with respect to base-shear strength, which enables an approximate assessment of buildings whose base-shear strength is outside the strength range included in this study. Although such normalization is not exact for buildings responding in the nonlinear range, studies have shown it to produce reasonable estimates of collapse probability within the range of strengths typical for such buildings (ATC 78, 2014)

Many older-type buildings will have been designed by allowable stress design methods. For this study, however, the buildings were designed using the strength design method as represented in ASCE 7-10 and ACI 318-11, so that the strengths can be understood from a modern design and assessment perspective. Load factors, resistance factors, and load combinations were in accordance with ASCE 7-10, except design for orthogonal effects and accidental torsion was not included.

For each building configuration (4, 8, or 12 stories), the structure initially was designed in accordance with the special moment frame requirements of ACI 318-11, except $\Sigma M_{nc}/\Sigma M_{nb} = 1.0$ at every joint except the roof level (ΣM_{nc} = sum of nominal moment strengths of columns at a beam-column joint and ΣM_{nb} = sum of nominal moment strengths of beams at the same joint).. Variations on this design were introduced (a) by reducing or increasing the beam moment strengths to achieve different relative moment strengths of beams and columns at beam-column joints, and (b) by varying the spacing of column transverse reinforcement to achieve different relative moment and shear strengths of columns, with transverse reinforcement spacing representative of the range for modern designs and older designs. Sums of ratios of column nominal moment strengths to beam nominal moment strengths had values $0.6 \leq \Sigma M_{nc}/\Sigma M_{nb} \leq 1.8$. Shear strength demand corresponding to development of column moment strength was calculated as $V_u = 1.2*(M_{n,top}+M_{n,bot})/l_u$, and initial nominal shear strength V_n of a column was calculated in accordance to ASCE 41-06 (2006) as

$$V_n = k\left[\frac{A_v f_{yt} d}{s} + \lambda\left(\frac{6\sqrt{f'_c}}{M/Vd}\right)\sqrt{\left(1+\frac{N_u}{6\sqrt{f'_c}A_g}\right)}0.8A_g\right], \quad (1)$$

in which k and λ was assumed to be equal to 1.0, A_v = transverse reinforcement area, f_{yt} = transverse reinforcement yield strength, s = center-to-center spacing of transverse reinforcement, f'_c = concrete compressive strength, d = effective depth, N_u = applied axial compressive force, and A_g = gross cross-sectional area. The transverse reinforcement was varied to achieve $0.6 \leq V_u/V_n \leq 1.2$. The versions of the frames with V_u/V_n =0.6 and $\Sigma M_{nc}/\Sigma M_{nb} = 1.2$ are referred to as the "modern code design" buildings.

Table 1 depicts all the various combinations that were considered in the current study. The individual building designs were set up such that a building had the same value of V_u/V_n in every story and the same value of $\Sigma M_{nc}/\Sigma M_{nb}$ at every joint (except the roof). Design requirements for beam-column joints and for other elements of the structural system were not considered.

Table 1. Combinations of V_u/V_n and $\Sigma M_{nc} / \Sigma M_{nb}$ considered in the current study (the shaded cell corresponds to modern building code design)

V_u/V_n \ $\Sigma M_{nc}/\Sigma M_{nb}$	**0.6**	**0.8**	**1.0**	**1.2**	**1.4**	**1.6**	**1.8**
0.6	√	√	√	√	√	√	√
0.8	√	√	√	√	√	√	√
1.0	√	√	√	√	√	√	√
1.2	√	√	√	√	√	√	√

Applying all the variations of Table 1 to 4, 8, and 12-story frames required 84 different designs. It was impractical to implement detailed designs for all the variations. Instead, the modern code design buildings were fully designed, and actual moment strengths were compared with required moment strengths. For typical members, the combination of resistance factors, code minimum reinforcement requirements, nominal member oversizing, and material overstrengths resulted in member expected strengths approximately 1.5 to 2.0 times required strengths, the factor depending on the number of stories in the frame. This factor was applied uniformly to all members in the frame to establish expected strengths, and then indicative longitudinal and transverse reinforcement was defined for each member. The indicative reinforcement was used to

define force-deformation relations for nonlinear analyses that would be carried out as part of this study.

NON-LINEAR SIMULATION MODELS

The idealized buildings described in the previous section were assumed to have symmetric plan, such that they respond to earthquake ground motion without plan torsion. To simplify the analysis approach, each building was modeled using a two-dimensional structural frame. Thus, biaxial interaction associated with simultaneous loading in two plan directions was not represented. The simulated frame for each studied building corresponds to an interior frame. This frame was assigned one-sixth of the total effective mass plus vertical loads associated with weight that was tributary to the frame. To account for non-linear geometry effects, a P-Delta formulation was employed.

The structural analysis model is an assemblage of line elements representing the flexibilities of beams and columns connected to beam-column joints and to fixed supports at a rigid foundation. To approximate flexibilities of beam-column joints, the joints were modeled with rigid dimensions equal to $d/2$, where d is the effective depth of the connected beam and column member. The diaphragm was modeled as rigid. For dynamic analyses, damping was assumed equal to 2% of critical damping, and was simulated using Rayleigh damping with parameters established so that damping was 2% of critical at the initial first- and third-mode periods.

As indicated in the previous section, the study considered a variety of designs of the same building configuration but with different spacing of transverse reinforcement. This results in different ratios of shear demand to shear capacity, V_u/V_n, such that failure of structural components could occur due to either flexure or shear. Following the ASCE 41-06 Supplement 1 procedures, it was assumed that shear failure is not likely to dominate member failure where $V_u/V_n < 0.7$. Thus, only flexural failure was modeled for this case. Where $V_u/V_n \geq 0.7$, the possibility of having shear failure or shear induced axial failure was also considered by explicitly modeling nonlinearities associated with flexural, shear, and axial failure. Nonlinearities associated with splice failures and beam-column joint failures were not modeled.

To model the non-linear flexural behavior of the structure, a concentrated plasticity approach was used for both beams and columns. By this approach, all the elements consisted of at least three parts: a linear elastic element and one rotational spring at each end. For those cases where shear and axial failure should be also considered according to the V_u/V_n ratio, a horizontal spring and a vertical spring were also connected in series with the linear elastic element to model shear and axial inelastic response, respectively. To enable the selection of parametric values related with strength and plasticity of structural members, indicative reinforcement was selected such that the provided strength resulted in values similar to the required strength, as indicated in the previous section. The modeling tools employed to model flexural, shear, and axial failure are described in more detail in Appendix A.

To account for concrete cracking and reinforcement slip from connections, the linear elastic elements had flexural, shear, and axial stiffness taken as a fraction of the gross-section stiffness in accordance with ASCE 41-06 Supplement 1. Using this model, the fundamental periods were 1.14s, 1.62s, and 1.95s for the 4, 8, and 12-story buildings, respectively.

Nonlinear static (pushover) analysis using an inverted triangular load pattern was performed for the three studied buildings having $V_u/V_n = 0.6$ and $\Sigma M_{nc}/ \Sigma M_{nb} = 1.2$, that is, flexure-controlled with code-required column to beam strength ratio. It is recognized that nonlinear static analysis does not accurately represent behavior expected under dynamic loading. It is used here only to define an index strength and drift capacity. Figure 3 plots relations between roof drift and base shear. Base-shear strengths range from approximately $0.13W$ to $0.2W$. Drift ratio capacities are higher for the shorter buildings, apparently because of localized yielding and P-delta effects that are more dominant in the taller buildings. As has been reported previously by Kuntz and Browning (2003) and others, the provision of $\Sigma M_{nc}/\Sigma M_{nb} = 1.2$ does not prevent formation of localized mechanisms that extend over only the lower stories. The calculated yield mechanisms under static loading extended through the second, third, and fourth stories of the 4, 8, and 12-story buildings in this study. Figure 4 shows displaced shapes at incipient failure of the studied buildings.

ASSESSMENT OF SEISMIC BEHAVIOR

Seismic behavior of the studied building models was assessed using the incremental dynamic analysis (IDA) method. According to this method, an analytical model of a building was subjected to numerous dynamic analyses under multiple ground motions scaled gradually to increasing acceleration amplitude. Collapse was defined for the smallest input motion required to achieve either one of the following two limit states: 1) Maximum inter-story drift ratio exceeding 10% of story-height, or 2) Shear or axial failure in more than 50% of the columns in any story. A suite of 22 pairs of far-field ground motions was selected, for a total of 44 ground motions. The same ground motions were used for FEMA P-695 (ATC-63). The output of the analysis is the relation between the spectral acceleration (at the first-mode period T_1 of the building) and maximum inter-story drift ratio for a given ground motion record.

Figure 5 shows a typical output from an IDA analysis of a single building. Each line in the figure represents the response of the building to a single ground motion record scaled to increasing intensity. Note that the curves begin to flatten out at maximum inter-story drift ratio of approximately 0.03 to 0.04, suggesting that the structure becomes unstable at around this inter-story drift ratio.

The collapse risk of each building model was obtained from statistics on the IDA results. In this study, collapse performance was evaluated using the probability of collapse as a function of the ground motion intensity level, defined in terms of $S_a(T_1)$. The collapse probabilities in terms of $S_a(T_1)$ were assumed to be log-normally distributed. Figure 6 shows collapse fragility relations. The interested reader could find a more detailed description the fragility curve development procedure in Appendix B.

The variation of structural parameters (beam moment strength and column transverse reinforcement) could lead to changes in the overall building strength. To avoid comparison bias that could occur due to differences in building strength, the results of the study were normalized with respect to the maximum base shear capacity of the frame V_{max}. The value of V_{max} was calculated from non-linear static analysis with inverted triangular load pattern. The new normalized strength parameter R_e defined as:

$$R_e = \frac{S_a(T_1) \times (W_{building} / g)}{V_{\max}}, \tag{2}$$

Note that R_e represents approximately the ratio of elastic demand to actual strength. It is not the same as the response modification coefficient R of ASCE 7-10, which is the ratio of the elastic demand for the design earthquake level to the required design strength.

Several approximations or simplifications in analysis have been noted, including planar frame analysis under horizontal ground motions only, frame elements with concentrated plasticity that does not account for overturning, and normalization of results using strengths obtained from nonlinear static analysis. Thus, the results cannot be expected to be accurate representations of real building performance. Nonetheless, the results provide important insight into the effects of different variables on collapse probability.

USING COLLAPSE INDICATORS TO PERFORM EARTHQUAKE RISK ASSESMENT FOR EXISTING BUIDLINGS

For buildings assigned to the highest Seismic Risk Categories and having moment frames as the seismic force-resisting system, ACI 318 requires that the moment frames be proportioned and detailed as special moment frames. For such frames, ACI 318-11 requires that the sum of column nominal moment strengths be at least 1.2 times the sum of beam nominal moment strengths at every beam-column joint. (Some localized exceptions to this requirement can be permitted.) This requirement is commonly referred to as the “strong-column, weak-beam” requirement. Its purpose is to promote beam yielding rather than column yielding, thereby spreading flexural yielding over multiple stories as the building responds to strong earthquake shaking. In buildings with relatively weak columns, column hinging may lead to deformations concentrated in one story, resulting in a so called weak-story mechanism. Older concrete buildings commonly do not satisfy the strong-column, weak-beam requirement, making them more vulnerable to damage and collapse.

To study the effect of column-to-beam strength ratio on the collapse risk of buildings with otherwise good details, the beam moment strengths were scaled to achieve column-to-beam moment strength ratios $\Sigma M_{nc}/\Sigma M_{nb}$ varying from 0.6 to 1.8. Transverse reinforcement was sufficient to result in V_u/V_n = 0.6, such that shear failures were

prevented in the study. Figure 7 presents partial results from the analyses, in this case plotting probability of collapse as a function of $\Sigma M_{nc}/\Sigma M_{nb}$ for R_e = 3. A notable observation is that there is rapid increase in collapse probability for values of $\Sigma M_{nc}/\Sigma M_{nb}$ less than approximately 1.2, the minimum value permitted by ACI 318-11 for special moment frames.

Figures 8 (a)-(c) depict the effect of $\Sigma M_{nc}/\Sigma M_{nb}$ for different values of the parameter R_e for the three building frames. Note that in this figure, all the buildings have closely spaced transverse reinforcement resulting in ductile flexural response without possibility of shear failure. From the figure, several observations can be made. In general, collapse probability increases as R_e increases. For values of $\Sigma M_{nc}/\Sigma M_{nb}$ = 1.2 and R_e = 3, probability of collapse is approximately 10% for the four-story frame, increasing to approximately 20% for the 12-story frame. Thus, to achieve the same probability of collapse, a larger value of $\Sigma M_{nc}/\Sigma M_{nb}$ is required for taller buildings than for shorter buildings.

Existing buildings commonly do not have closely spaced transverse reinforcement, making them more susceptible to shear and axial failures. To study this effect, the spacing of column transverse reinforcement was varied in each of the building models to achieve values of V_u/V_n ranging from 0.6 to 1.2. For each value of V_u/V_n, ratios of column-to-beam moment strengths $\Sigma M_{nc}/\Sigma M_{nb}$ were varied from 0.6 to 1.8, creating a full matrix of results for the range of V_u/V_n and $\Sigma M_{nc}/\Sigma M_{nb}$. For frames having $V_u/V_n > 0.7$, shear and axial failure was considered a possibility. Therefore, for these frames, the analytical model was modified to enable simulation of shear and axial failures. Additional details regarding the analytical modeling approach are provided by Galanis and Moehle (2013).

Incremental dynamic analyses were conducted for each combination of the study variables. Figure 9 presents collapse fragility curves evaluated from the incremental dynamic analysis results. The figure conveys information that can be interpreted in different ways. For example, for a given value of R_e, the collapse fragility is much higher for the frames with shear-critical columns than for frames with flexure-controlled columns. Alternatively, for a building with shear-critical columns to have the same

collapse fragility as a frame with flexure-controlled columns, it must have higher base-shear strength (that is, smaller R_e).

Figure 10 compares the effect of V_u/V_n for the 4, 8, and 12-story frames, in each case for $\Sigma M_{nc}/\Sigma M_{nb}$ = 1.2 and R_e = 3. For each configuration, the collapse probability increases as the transverse reinforcement spacing increases (that is, V_u/V_n increases). Also, for a given value of V_u/V_n, a taller building is always more vulnerable than a shorter one. This is because shear failure generally is restricted to a single story, such that most of the building lateral drift concentrates in that story. In a tall building, a single-story failure represents a more severe localization and therefore higher demand than occurs in an otherwise identical shorter building. P-delta effects also are greater for a taller building, exacerbating strength loss and thereby accelerating failure.

Figure 11 presents collapse probability results for the complete matrix of V_u/V_n and $\Sigma M_{nc}/\Sigma M_{nb}$ values that were investigated for the 8-story building. Collapse probabilities increase with increasing R_e, increasing V_u/V_n, and decreasing $\Sigma M_{nc}/\Sigma M_{nb}$. The combination of low strength, high V_u/V_n, and low $\Sigma M_{nc}/\Sigma M_{nb}$ is especially critical. Similar results were obtained for the 4- and 12-story frames.

Figure 12 presents collapse probability results for the complete matrix of V_u/V_n and $\Sigma M_{nc}/\Sigma M_{nb}$ values for 4, 8, and 12-story frames. A list of probability of collapse values for all the considered cases in a matrix format is presented in Appendix D.

As previously noted, collapse probabilities increase with increasing V_u/V_n, and decreasing $\Sigma M_{nc}/\Sigma M_{nb}$. The combination of low strength, high V_u/V_n, and low $\Sigma M_{nc}/\Sigma M_{nb}$ is especially critical, and more-so for taller frames than for shorter frames. For the flexure-controlled frames (Figure 12a), collapse probabilities increase significantly for $\Sigma M_{nc}/\Sigma M_{nb}$ less than approximately 1.2 (the required value in ACI 318-11 for special moment frames). For frames with shear-critical columns (Figure 12 b, c, and d), the critical value of $\Sigma M_{nc}/\Sigma M_{nb}$ appears to shift to higher values.

CONCLUSIONS

An analytical study explored the collapse risk posed by reinforced concrete building frames having different design characteristics. The study was mainly interested in identifying characteristics that correlated with high collapse risk. Such information could

be useful as an aid to identifying buildings with the highest risk. The analytical study considered the effects of three structural parameters, specifically, ratios of column to beam moment strengths at beam-column joints ($\Sigma M_{nc}/\Sigma M_{nb}$), ratios of column shear demands to column shear capacities (V_u/V_n), and number of stories. The selected parameters are easily determined without performing any complicated analysis and therefore could serve as useful parameters for quickly assessing the collapse potential of an existing building. Effects of irregular configurations or strength distributions, effects of plan torsion, and effects of structural walls including infills were not included in the study. Within the limits of the study, the following conclusions are made:

1. Ground motion intensity was measured by the linear, 2%-damped, response spectral acceleration at fundamental vibration period of a frame. For any of the frames studied, the ground motion intensity required to cause collapse varied significantly from one ground motion to another. Thus, using this ground motion intensity measure, collapse risk must be assessed probabilistically.

2. For regular frames of the type considered in this study, having reasonable values of the variable $\Sigma M_{nc}/\Sigma M_{nb}$, beam yielding mechanisms do not extend full height but instead are concentrated in the lower stories. For the case of $\Sigma M_{nc}/\Sigma M_{nb} = 1.2$, about one-quarter of the building height participates in the collapse mechanism while for the case of $\Sigma M_{nc}/\Sigma M_{nb} = 1.6$ the percentage increases to 30-60%.

3. For frames detailed to have flexural ductility without shear failure, the probability of collapse decreased with increasing values of the variable $\Sigma M_{nc}/\Sigma M_{nb}$. The greatest percentage reduction in collapse probability occurred for $\Sigma M_{nc}/\Sigma M_{nb}$ in the range 1.0 to 1.4. The ACI Building Code (ACI 318-11) requires $\Sigma M_{nc}/\Sigma M_{nb} \geq 1.2$, which compares favorably with the range of maximum benefit found in this study.

4. For a given base-shear coefficient, taller frames are more likely to collapse than shorter frames because of the tendency of collapse mechanisms to concentrate in relatively fewer stories and because of *P*-delta effects.

5. For all other variables being the same, the collapse probability increases with increasing values of the variable V_u/V_n, that is, as columns become increasingly shear-critical.

6. All the variables considered in this study (building height, effective strength coefficient R_e, $\Sigma M_{nc}/\Sigma M_{nb}$, and V_u/V_n) interact, such that it is necessary to consider the combination of variables in order to quantify the collapse probability.

ACKNOWLEDGMENTS

The work presented here was supported by the Federal Emergency Management Agency through the Applied Technology Council (ATC-78 project). Additional financial support for the first writer has been provided by the Fulbright Foundation, International Science and Technology Award, and by the U.S. National Science Foundation under Award 0618804. The writers appreciate the participation and invaluable contributions of collaborators from the ATC-78 project, including Kenneth Elwood, Robert Hanson, John Heintz, William Holmes, Jon Kiland, Abbie Liel, Mike Mehrain, Chris Rojahn, Siamak Sattar, and Peter Somers.

REFERENCES

ACI 318-11 (2011), *Building Code Requirements for Structural Concrete (ACI 318-11) and Commentary*, American Concrete Institute.

ASCE 7-10 (2010), *Minimum Design Loads for Buildings and Other Structures*, American Society of Civil Engineers.

ASCE 41-06 (2006), *Seismic Rehabilitation of Existing Buildings*, (with Supplement 1), American Society of Civil Engineers.

ASCE 31-03 (2003), *Seismic Evaluation of Existing Buildings*, American Society of Civil Engineers.

ATC 78 (2014), *Evaluation of the Methodology to Select and Prioritize Collapse Indicators in Older Concrete Buildings, FEMA. (in-press)*

EERI (2011). "The Concrete Coalition and the California Inventory Project: An Estimate of the Number of Pre-1980 Concrete Buildings in the State," Earthquake Engineering Research Institute, available as

https://www.eeri.org/wpcontent/uploads/Concrete_Coalition_Final_0911.pdf.

Elwood, K.J. (2004), "Modelling Failures in Existing Reinforced Concrete Columns," *Canadian Journal of Civil Engineering*, 37:5, 846-859

Elwood, K.J. and Moehle, J.P. (2008), "Dynamic Collapse Analysis for a Reinforced Concrete Frame Sustaining Shear and Axial Failures," *Earthquake Engineering and Structural Dynamics*, 37:1, 991-1012.

Elwood, K.J. and Moehle, J.P. (2005a), "Drift Capacity of Reinforced Concrete Columns with Light Transverse Reinforcement," *Earthquake Spectra*, 21:1, 71-89.

Elwood, K.J. and Moehle, J.P. (2005b), "Axial Capacity Model for Shear-Damaged Columns," *ACI Structural Journal*, 102:4, 578-587.

Galanis, P.H., Moehle, J.P (2012), "Development of Collapse Indicators for Older-Type Reinforced Concrete Buildings," *15th World Conference on Earthquake Engineering, Lisboa 2012*.

Haselton, C.B. , Liel, A.B, Lange, S. and Deierlein, G.G. (2007*),* "Beam-Column Element Model Calibrated for Predicting Flexure Response Leading to Global Collapse of RC frame Buildings," PEER Report 2007/03, Pacific Earthquake Engineering Research Center, University of California, Berkeley.

Haselton, C.B., Liel, A.B. , Deierlein, G.G. , Dean B.S. and Chou J.H (2011), "Seismic Collapse Safety of Reinforced Concrete Buildings. II: Assessment of Ductile Moment Frames," *Journal of Structural Engineering*,137:4, 481-491.

Ibarra, L.F., Medina, R.A. and Krawinkler, H. (2005), "Hysteretic Models that Incorporate Strength and Stiffness Deterioration," *Earthquake Engineering and Structural Dynamics*, 34:12, 1489-1511.

Kuntz, G.L. and Browning J. (2003), "Reduction of Column Yielding During Earthquakes for Reinforced Concrete Frames," *ACI Structural Journal*, 100:5, 573-580.

Liel, A.B., Haselton, C.B. and Deierlein, G.G. (2011), "Seismic Collapse Safety of Reinforced Concrete Buildings. II: Comparative Assessment of Nonductile and Ductile Moment Frames," *Journal of Structural Engineering*, 137:4, 492-502.

NEHRP Consultants Joint Venture (2010), "Program Plan for the Development of Collapse Assessment and Mitigation Strategies for Existing Reinforced Concrete Buildings," National Institue of Standards and Technology, Washington, D.C.

UBC (1976). *Uniform Building Code*, International Council of Building Officials.

Vamvatsikos, D. and Cornell, C.A. (2004), "Applied Incremental Dynamic Analysis," *Earthquake Spectra*, 20:2, 523-553

APPENDIX A: MODELING TECHNIQUES

Two sources of nonlinearity were considered explicitly in the nonlinear analyses: (a) inelastic flexure, and (b) inelastic shear and shear-induced axial failure. For beams, only inelastic flexure was modeled; for columns, both failure modes were simulated. Currently available software and modeling knowledge does not readily provide for a smooth transition between these two failure modes. For this reason, consistent with the modeling procedures in ASCE 41-06, flexural failures were assumed to predominate where $V_u/V_n < 0.7$, and shear and axial failures were assumed to predominate where $V_u/V_n \geq 0.7$.

For the case of $V_u/V_n < 0.7$, non-linear flexural response was modeled using the concentrated plasticity approach. According to this approach a line element with mechanical properties that represent the linear-elastic flexural response of the structural member is employed to connect two plastic hinges located at the ends. Figure A-1 illustrates the concentrated plasticity approach.

The nonlinear rotational springs were based on the Clough model, using hysteresis implemented in OpenSees by Ibarra et al. (2005). This model uses a post-capping negative slope to model strain-softening behavior associated with degradation of the flexural resisting mechanism (due to concrete crushing, reinforcement buckling, reinforcement fracture, and interaction with shear). The model also incorporates cyclic strength degradation. .

This element model requires the specification of seven parameters to control the monotonic and cyclic behavior of the model, specifically, M_y, M_c/M_y, $\theta_{cap,pl}$, θ_{pc}, λ, and c. The value of M_y (nominal moment strength) was determined analytically using the ACI 318-11 (2011) code provisions while the ratio M_c/M_y was assumed to be equal to 1.2. The values of λ, c, $\theta_{cap,pl}$ and θ_{pc} were calculated according to equations similar to the ones presented in Haselton et al. but re-calibrated to exclude those cases in the column database used by Haselton (2007) for which shear or flexure-shear failure were reported. (It should be noted that the dissipation capacity term λ as appears in Haselton et al. is different from the λ parameter used in equation 2 to estimate the shear strength of column members.) The recalibrated relationships are presented in Appendix C. Figures A-2 and A-3 depict the behavior of the nonlinear rotational springs for a representative column.

For the cases where $V_u/V_n > 0.7$, it is possible that shear failure will occur, possibly followed by axial failure. The model presented in Elwood and Moehle (2008) was used to simulate this behaviour. Flexural response is modelled using a lumped plasticity model (linear-elastic line element plus plastic hinges at the member ends), similar to the model used for flexure-controlled behaviour. Two additional springs are added at the top of each column member to model shear and axial failure (Figure A-4).

As explained by Elwood (2004), the flexural behaviour of the plastic hinges must always maintain a positive slope in order to avoid convergence problems and to ensure localization of damage in the shear spring. Thus, the parameters $\theta_{,pc}$ of the connected rotational springs element are modified such that in-cycle flexural degradation is avoided. The remaining parameters maintain the values originally estimated for the case of $V_u/V_n \leq 0.7$.

The shear spring is linearly-elastic until the element detects the onset of shear failure. Thereafter, the shear spring follows a linear degrading branch. The onset of shear failure is defined as a function of the inter-story drift ratio of the column, as described in Elwood and Moehle (2008). As presented in Elwood and Moehle (2008), shear failure can only occur after the onset of flexural yielding. The model was updated for the present work such that shear failure could be initiated prior to flexural yielding. For this purpose, the model checks at every instance whether the applied shear exceeds the initial shear strength according to ASCE 41-06 (2006) as provided in Equation 1. If it does for any

instance, shear failure initiates, with subsequent behavior according to the Elwood and Moehle model.

APPENDIX B: DEVELOPMENT OF FRAGILITY CURVES

Incremental Dynamic Analysis (IDA) was used as described in the main body of this paper. A single-record IDA provides a single measure of how collapse occurs for that one ground motion record. To measure the variability in the dynamic response, multiple IDA analyses are done using different ground motions. Performing IDA analysis can be potentially resource intensive due to the large number of non-linear analyses required. To reduce the computational cost, the algorithm developed by Vamvatsikos (2001) was deployed.

After the IDA procedure has been completed, post-processing of the results is required in order to develop the fragility curve of the specified model. First the Empirical Cumulative Distribution Function (CDF) of probability of collapse as a function of ground motion intensity is drawn as shown in Figure B-1, using data points from the IDA. Then, following the procedure of FEMA-P695 (FEMA 2009), a lognormal distribution is fit to the collapse data points (Figure B-1). The lognormal collapse fragility is defined by two parameters, which are the logarithmic mean (μ_{ln}) and the standard deviation (σ_{ln}).

It should be noted that this study considered only the record-to-record collapse (aleatory) uncertainty. Modeling (epistemic) uncertainties where not considered. Also the effect of spectral shape of the considered ground motions in the estimation of the probability of collapse was not considered.

APPENDIX C: RECALIBRATION OF HASELTON ET AL. FLEXURAL MODEL PARAMETERS

The current study used the equations provided in Haselton et al. (2007) to define the structural parameters of the flexural failure models (V_u/V_n=0.6). As such, it was decided to recalibrate the coefficients of the model to exclude data for which $V_p/V_n > 0.7$ and for which flexure-shear failure was reported. The recalibration was performed by Dr. A. Liel and the results were provided to the authors as personal communication.

The updated equations used in the current study are cited below:

Equation for Plastic Rotation Capacity

Original

$$\theta_{cap,pl} = (0.13)(1+0.55a_{sl})(0.13)^{v}(0.02+40\rho_{sh})^{0.65}(0.99412)^{f'_c}, \quad (3)$$

Revised

$$\theta_{cap,pl} = (0.13)(1+0.55a_{sl})(0.16)^{v}(0.02+40\rho_{sh})^{0.55}(0.99412)^{f'_c}, \quad (4)$$

Equation for Post-Capping Rotation Capacity

Original

$$\theta_{pc} = (0.176)(0.031)^{v}(0.02+40\rho_{sh})^{1.02}, \quad (5)$$

Revised

$$\theta_{pc} = (1.13)(0.018)^{v}(0.02+40\rho_{sh})^{1.14}, \quad (6)$$

Equation for Cyclic Deteriotation

Original

$$\lambda = (170.7)(0.27)^{v}(0.10)^{s/d}, \tag{7}$$

Revised

$$\lambda = (189)(0.23)^{v}(0.10)^{s/d}, \tag{8}$$

Compared with the original equations, the recalibrated equations show increased in plastic rotation capacity, post-capping rotation capacity, and energy dissipation capacity.

APPENDIX D: COLLAPSE RISK TABLE OF THE STUDIED BUILDINGS

- **4-Story Building**

Table D.1 Probability of Collapse Matrix for the 4-story Building with V_u/V_n=0.6

R_e / $\Sigma M_{nc}/\Sigma M_{nb}$	**2**	**3**	**4**	**5**	**6**
0.6	0.02	0.18	0.44	0.68	0.83
0.8	0.02	0.19	0.45	0.68	0.83
1	0.02	0.15	0.39	0.62	0.79
1.2	0.00	0.06	0.19	0.36	0.54
1.4	0.00	0.03	0.11	0.24	0.37
1.6	0.00	0.01	0.04	0.12	0.25
1.8	0.00	0.01	0.03	0.10	0.19

Table D.2 Probability of Collapse Matrix for the 4-story Building with V_u/V_n=0.8

R_e / $\Sigma M_{nc}/\Sigma M_{nb}$	**2**	**3**	**4**	**5**	**6**
0.6	0.08	0.40	0.70	0.88	0.95
0.8	0.09	0.40	0.71	0.88	0.95
1	0.08	0.40	0.70	0.88	0.95
1.2	0.03	0.21	0.47	0.69	0.83
1.4	0.02	0.10	0.26	0.44	0.60
1.6	0.01	0.05	0.15	0.29	0.44
1.8	0.00	0.02	0.08	0.17	0.29

Table D.3 Probability of Collapse Matrix for the 4-story Building with V_u/V_n=1.0

R_e / $\Sigma M_{nc}/\Sigma M_{nb}$	**2**	**3**	**4**	**5**	**6**
0.6	0.18	0.58	0.84	0.95	0.98
0.8	0.17	0.58	0.84	0.95	0.98
1	0.16	0.54	0.81	0.93	0.98
1.2	0.05	0.31	0.61	0.81	0.92
1.4	0.02	0.16	0.38	0.59	0.75
1.6	0.01	0.08	0.22	0.38	0.54
1.8	0.00	0.03	0.11	0.24	0.39

Table D.4 Probability of Collapse Matrix for the 4-story Building with V_u/V_n=1.2

R_e / $\Sigma M_{nc}/\Sigma M_{nb}$	**2**	**3**	**4**	**5**	**6**
0.6	0.68	0.82	0.94	0.98	1.00
0.8	0.68	0.83	0.94	0.98	1.00
1	0.67	0.81	0.93	0.97	1.00
1.2	0.23	0.55	0.80	0.90	0.99
1.4	0.03	0.22	0.52	0.75	0.89
1.6	0.01	0.11	0.30	0.51	0.68
1.8	0.01	0.06	0.19	0.35	0.50

- **8-Story Building**

Table D.5 Probability of Collapse Matrix for the 8-story Building with V_u/V_n=0.6

R_e / $\Sigma M_{nc}/\Sigma M_{nb}$	2	3	4	5	6
0.6	0.10	0.43	0.73	0.89	0.96
0.8	0.10	0.44	0.74	0.89	0.96
1	0.09	0.37	0.65	0.82	0.92
1.2	0.02	0.14	0.35	0.56	0.72
1.4	0.00	0.03	0.14	0.32	0.50
1.6	0.00	0.01	0.08	0.21	0.37
1.8	0.00	0.01	0.06	0.15	0.29

Table D.6 Probability of Collapse Matrix for the 8-story Building with V_u/V_n=0.8

R_e / $\Sigma M_{nc}/\Sigma M_{nb}$	2	3	4	5	6
0.6	0.31	0.68	0.88	0.95	0.98
0.8	0.33	0.69	0.88	0.96	0.98
1	0.31	0.67	0.86	0.95	0.98
1.2	0.08	0.33	0.58	0.76	0.87
1.4	0.02	0.13	0.34	0.55	0.72
1.6	0.00	0.06	0.20	0.38	0.56
1.8	0.00	0.03	0.13	0.28	0.44

Table D.7 Probability of Collapse Matrix for the 8-story Building with V_u/V_n=1.0

R_e / $\Sigma M_{nc}/\Sigma M_{nb}$	2	3	4	5	6
0.6	0.46	0.83	0.95	0.99	1.00
0.8	0.45	0.82	0.95	0.99	1.00
1	0.41	0.78	0.93	0.98	0.99
1.2	0.13	0.44	0.70	0.86	0.93
1.4	0.03	0.21	0.47	0.68	0.82
1.6	0.02	0.12	0.32	0.52	0.69
1.8	0.00	0.06	0.20	0.39	0.57

Table D.8 Probability of Collapse Matrix for the 8-story Building with V_u/V_n=1.2

R_e / $\Sigma M_{nc}/\Sigma M_{nb}$	**2**	**3**	**4**	**5**	**6**
0.6	0.70	0.93	0.99	1.00	1.00
0.8	0.67	0.92	0.98	0.99	1.00
1	0.65	0.93	0.99	1.00	1.00
1.2	0.23	0.64	0.87	0.96	0.99
1.4	0.10	0.37	0.62	0.79	0.89
1.6	0.02	0.16	0.40	0.62	0.78
1.8	0.01	0.09	0.27	0.49	0.67

- **12-Story Building**

Table D.9 Probability of Collapse Matrix for the 12-story Building with V_u/V_n=0.6

R_e / $\Sigma M_{nc}/\Sigma M_{nb}$	2	3	4	5	6
0.6	0.12	0.55	0.85	0.96	0.99
0.8	0.12	0.54	0.85	0.96	0.99
1	0.08	0.45	0.79	0.93	0.98
1.2	0.03	0.24	0.56	0.79	0.91
1.4	0.00	0.08	0.30	0.55	0.75
1.6	0.00	0.04	0.18	0.40	0.62
1.8	0.00	0.03	0.14	0.32	0.52

Table D.10 Probability of Collapse Matrix for the 12-story Building with V_u/V_n=0.8

R_e / $\Sigma M_{nc}/\Sigma M_{nb}$	2	3	4	5	6
0.6	0.52	0.89	0.98	1.00	1.00
0.8	0.52	0.89	0.98	1.00	1.00
1	0.44	0.85	0.97	0.99	1.00
1.2	0.09	0.44	0.75	0.91	0.97
1.4	0.02	0.18	0.48	0.73	0.87
1.6	0.00	0.09	0.32	0.58	0.78
1.8	0.00	0.06	0.23	0.46	0.66

Table D.11 Probability of Collapse Matrix for the 12-story Building with V_u/V_n=1.0

R_e / $\Sigma M_{nc}/\Sigma M_{nb}$	2	3	4	5	6
0.6	0.65	0.93	0.99	1.00	1.00
0.8	0.65	0.93	0.99	1.00	1.00
1	0.56	0.91	0.99	1.00	1.00
1.2	0.16	0.60	0.87	0.96	0.99
1.4	0.05	0.33	0.65	0.85	0.94
1.6	0.01	0.17	0.46	0.72	0.87
1.8	0.01	0.11	0.35	0.61	0.79

Table D.12 Probability of Collapse Matrix for the 12-story Building with V_u/V_n=1.2

R_e / $\Sigma M_{nc}/\Sigma M_{nb}$	**2**	**3**	**4**	**5**	**6**
0.6	0.80	0.98	1.00	1.00	1.00
0.8	0.82	0.98	1.00	1.00	1.00
1	0.69	0.96	1.00	1.00	1.00
1.2	0.31	0.74	0.93	0.98	1.00
1.4	0.10	0.48	0.80	0.93	0.98
1.6	0.04	0.29	0.61	0.83	0.93
1.8	0.02	0.16	0.44	0.69	0.85

FIGURES

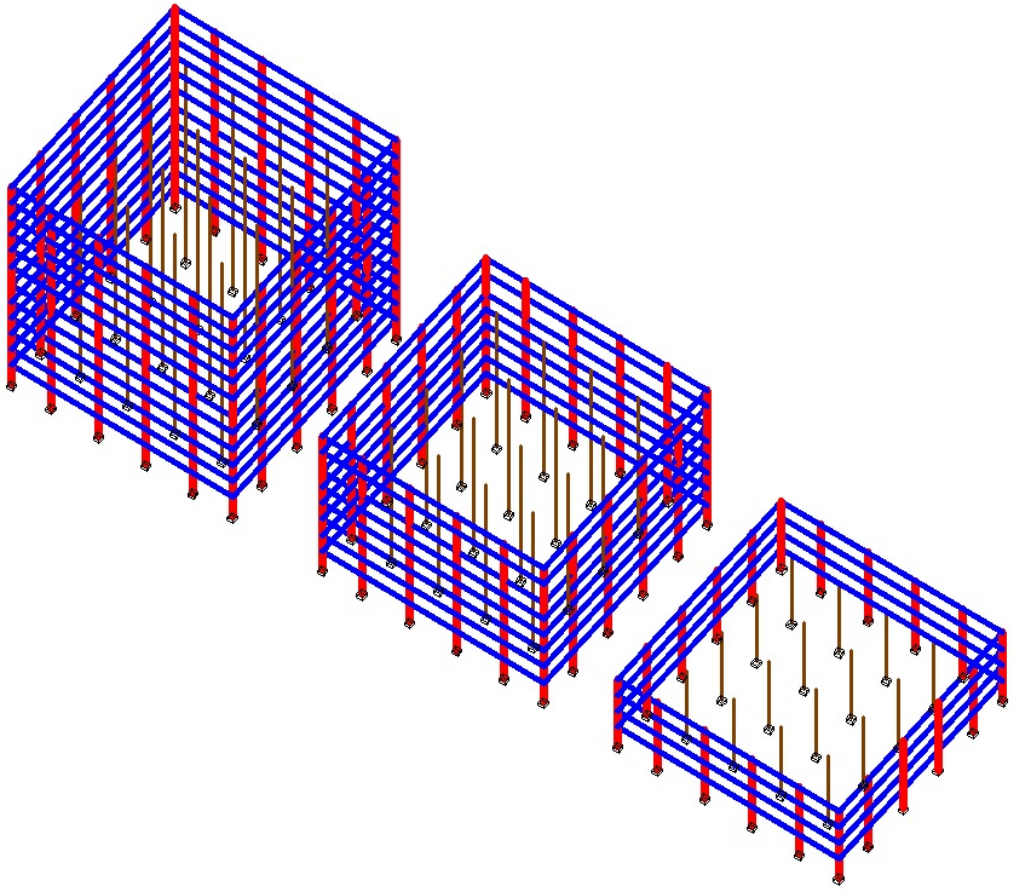

Figure 1. Three- dimensional view of the studied buildings (for clarity of presentation, only the perimeter frames are shown)

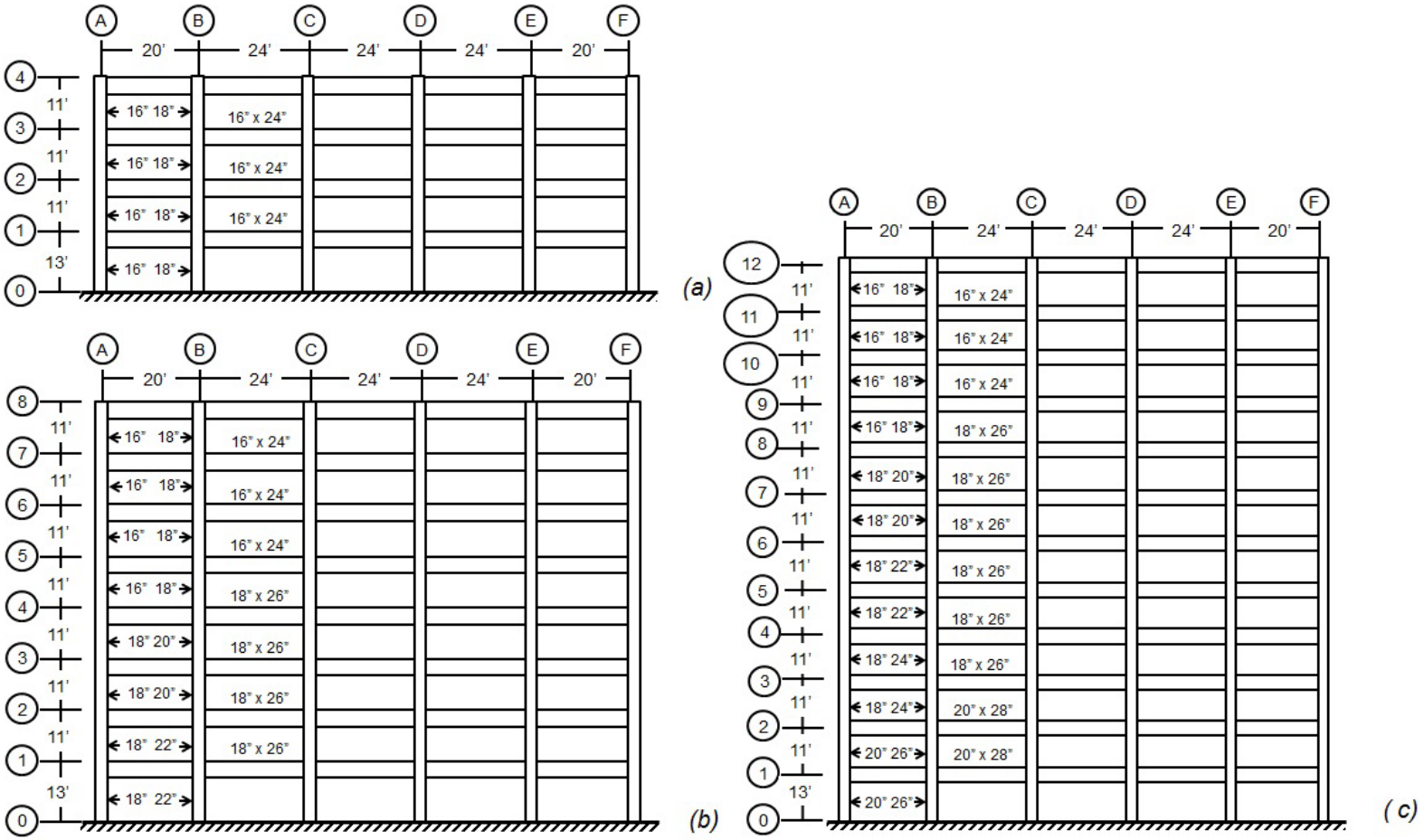

Figure 2. Schematic elevation view of the simulated frames: (a) 4-Story, (b) 8-Story, and (c) 12-Story buildings

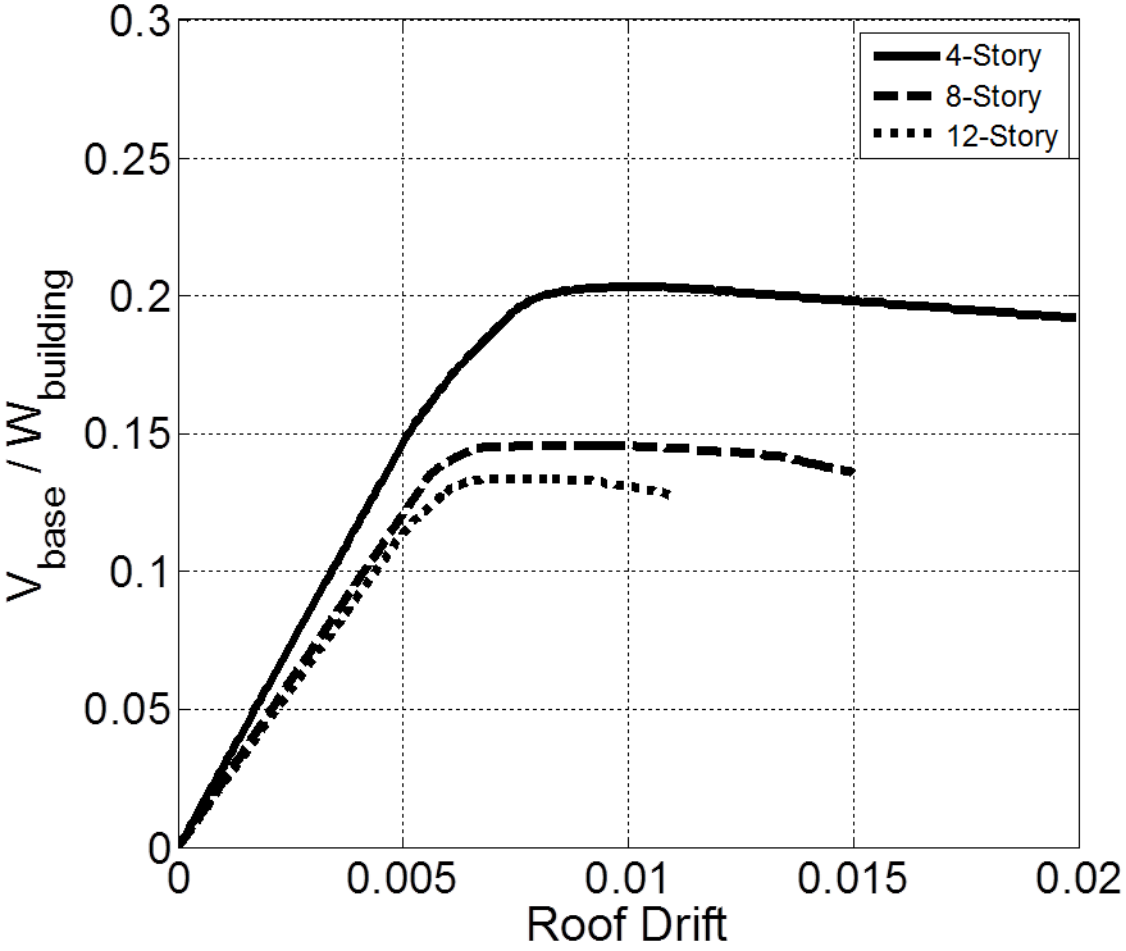

Figure 3. . Pushover analysis of the three "modern code design" building models" (V_u/V_n=0.6, $\Sigma M_{nc}/\ \Sigma M_{nb}$=1.2)

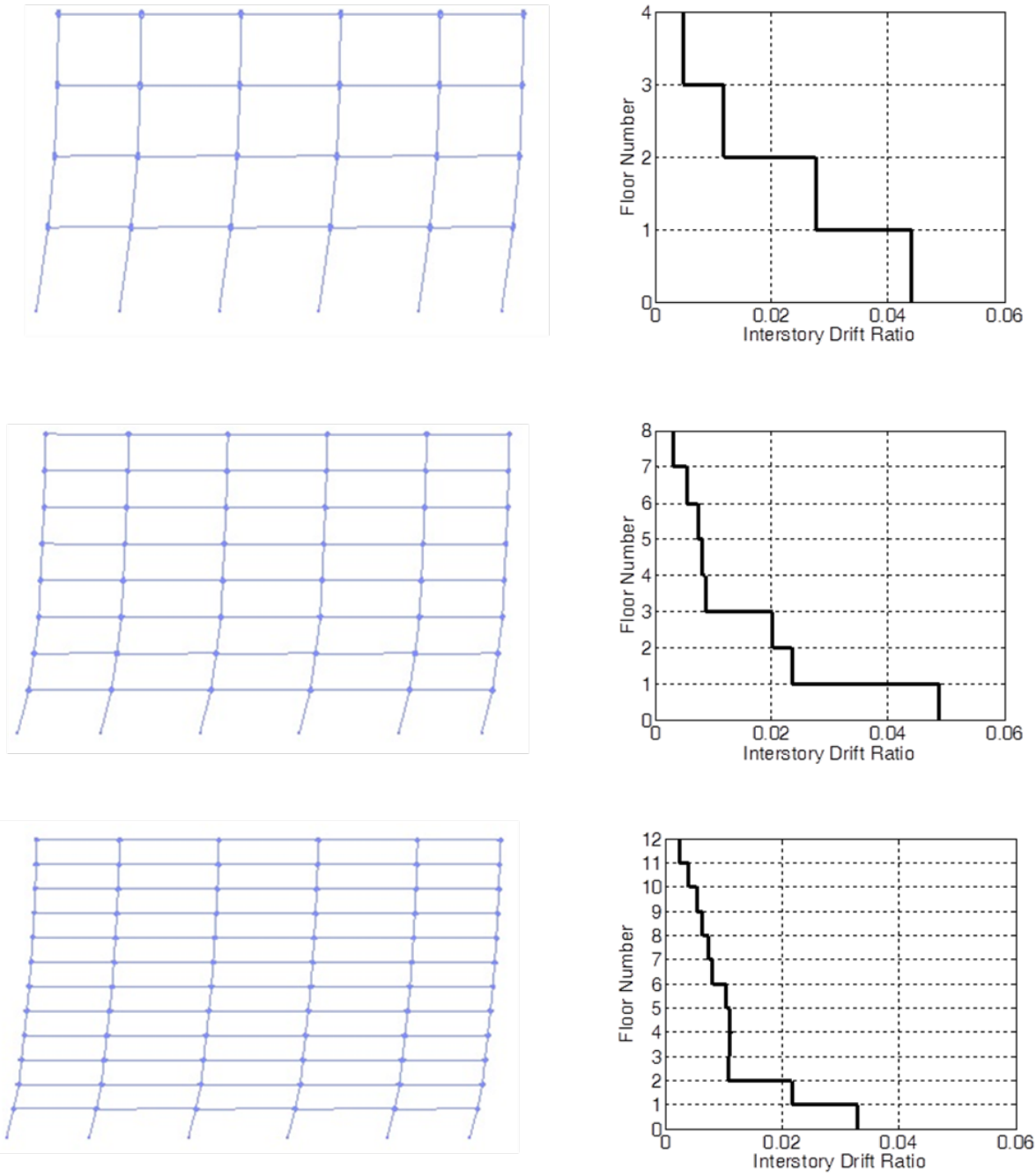

Figure 4. . Pushover analysis of the three "modern code design" building models (V_u/V_n=0.6, $\Sigma M_{nc}/\ \Sigma M_{nb}$=1.2)

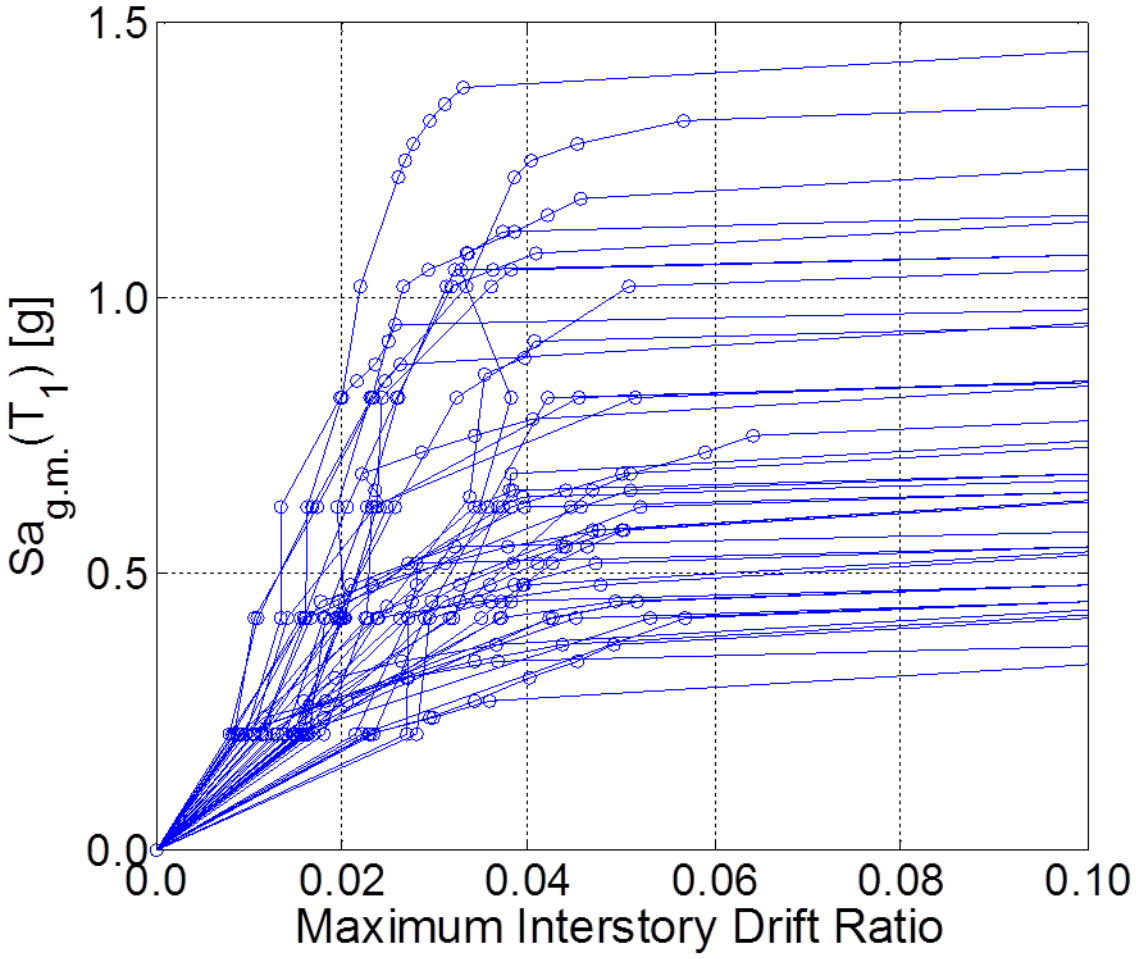

Figure 5. Incremental Dynamic Analysis (IDA) curves for the 8-story modern code design building model (V_u/V_n=0.6, $\Sigma M_{nc}/\ \Sigma M_{nb}$=1.2)

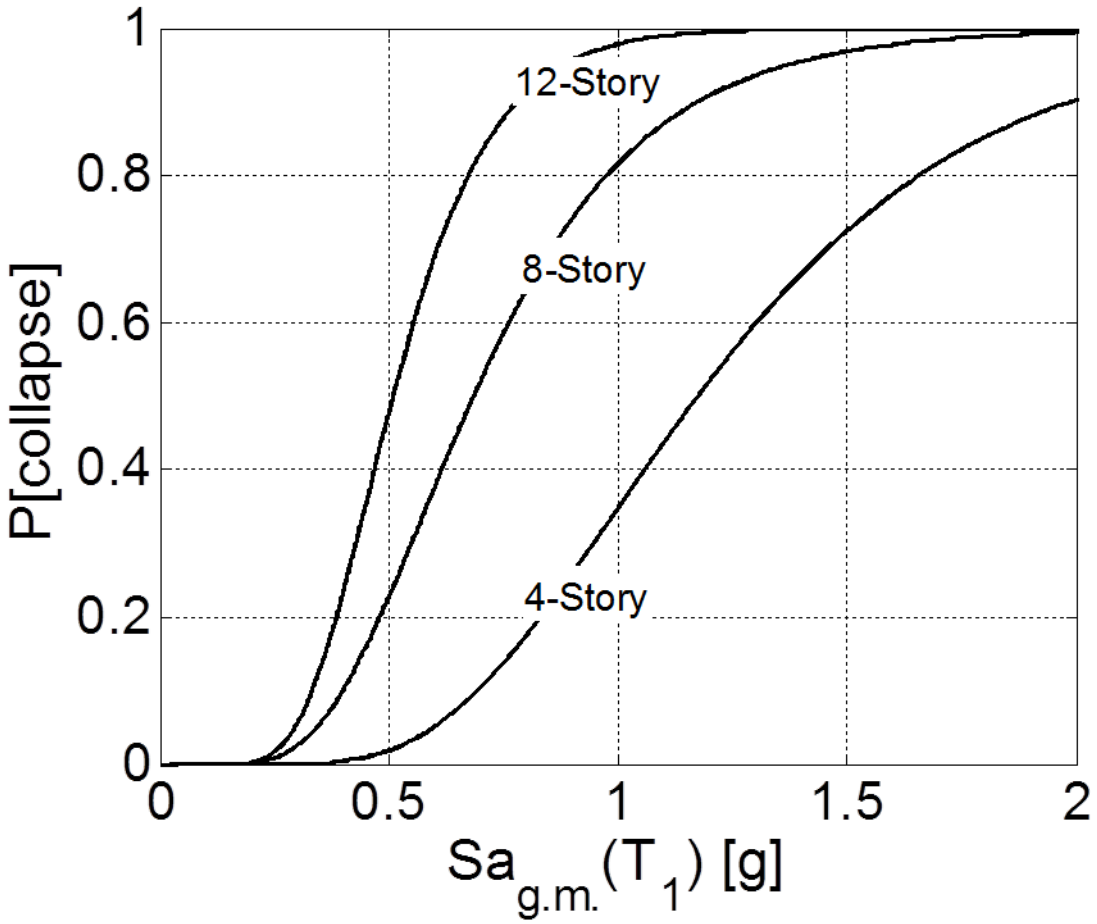

Figure 6. Collapse fragility functions for the "modern code design" building models (V_u/V_n=0.6, $\Sigma M_{nc}/\ \Sigma M_{nb}$=1.2)

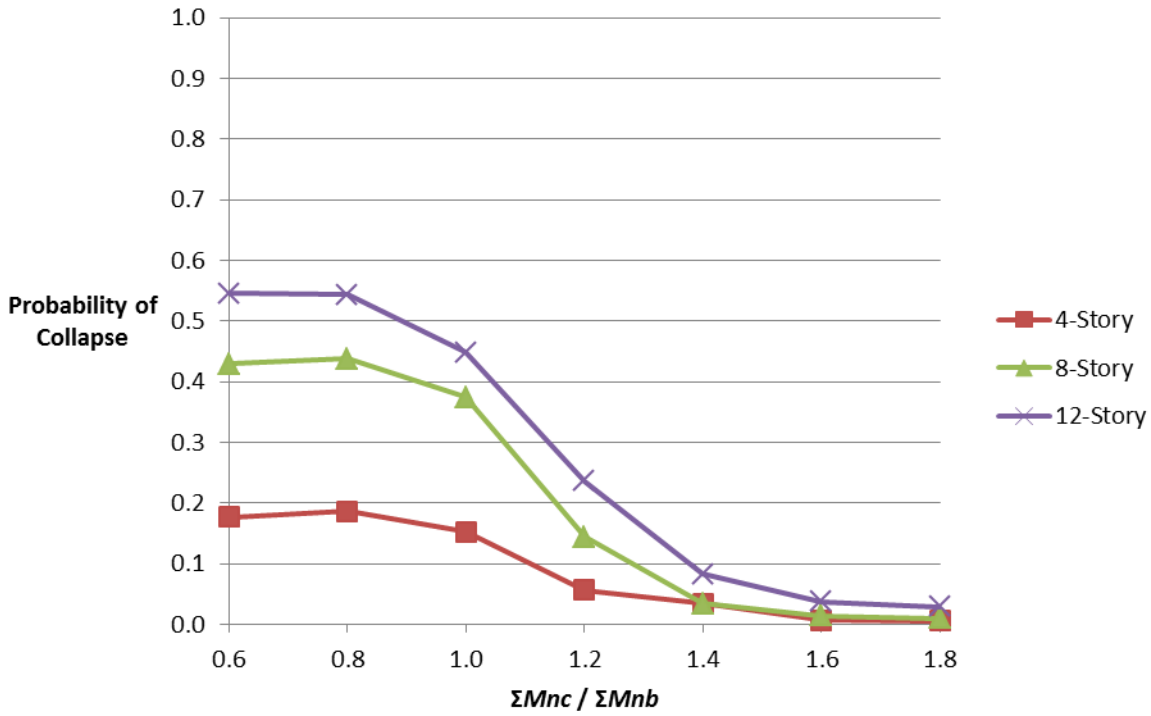

Figure 7. Comparison of collapse performance of the studied building models for R_e = 3 and V_u/V_n = 0.6

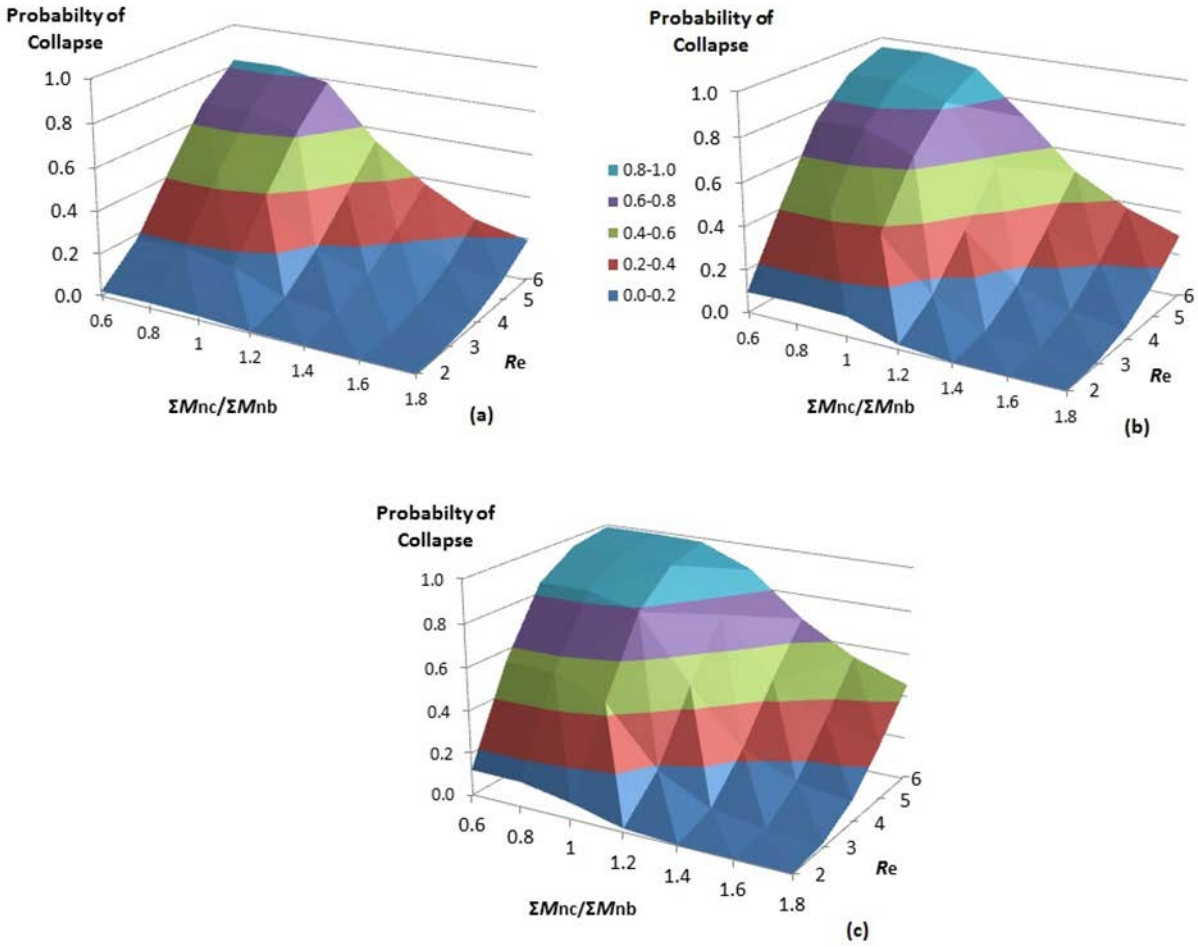

Figure 8. Collapse performance of (a) 4-story, (b) 8-story and (c) 12-story buildings with $V_u/V_n = 0.6$

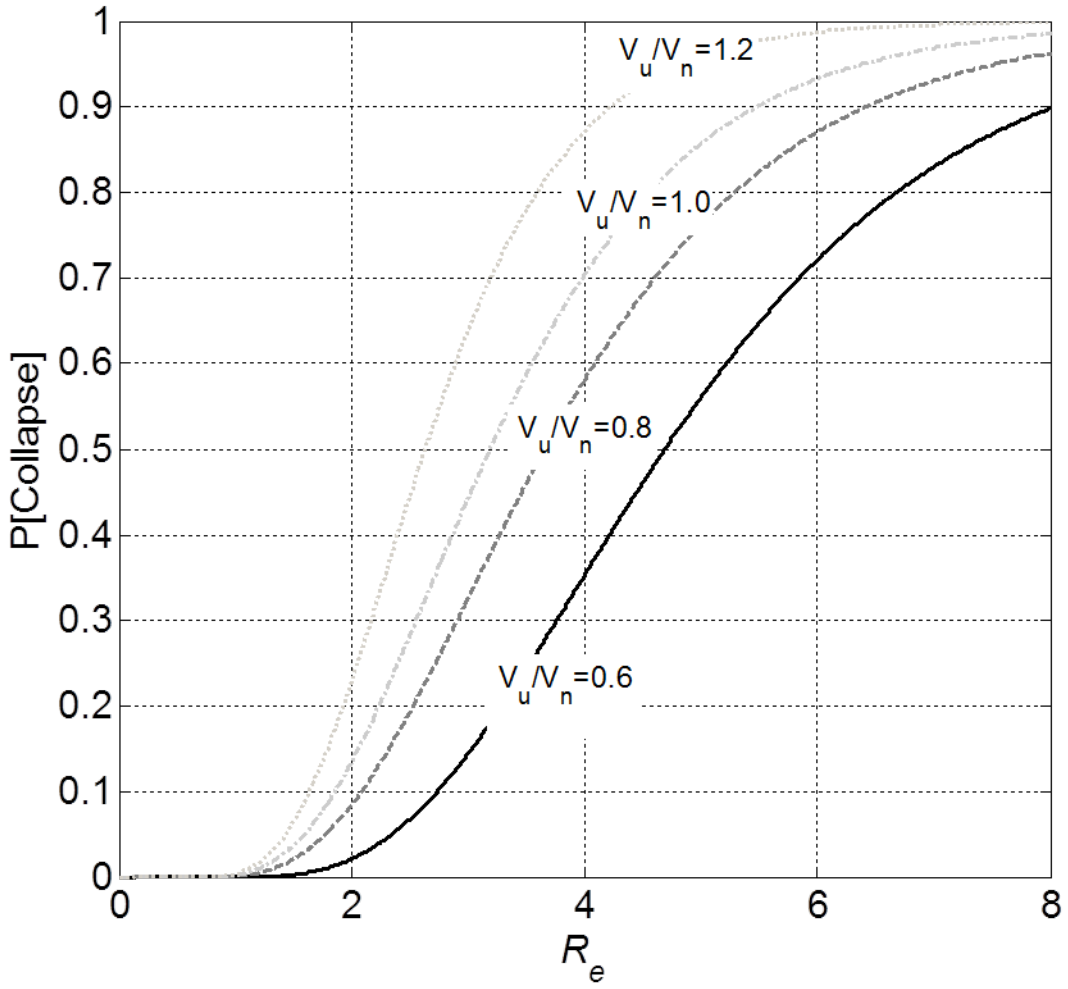

Figure 9. Comparison of the fragility curves of the 8-story building having $\Sigma M_{nc}/\Sigma M_{nb} = 1.2$

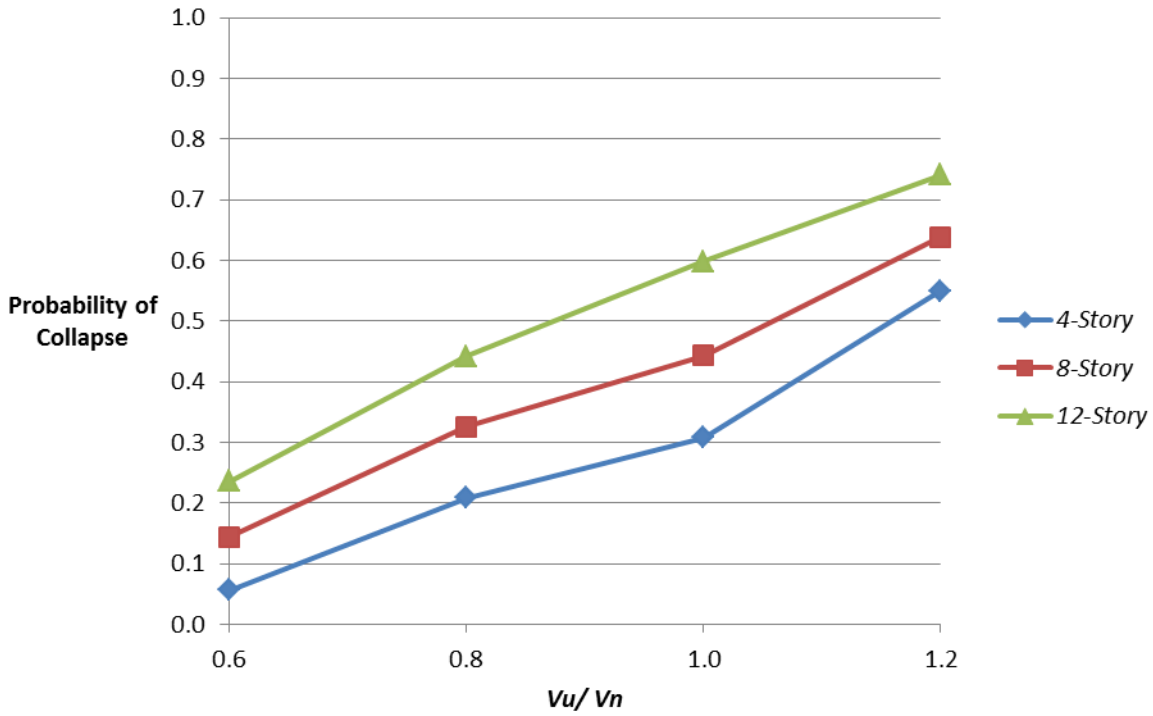

Figure 10. Comparison of the collapse performance of the three buildings for $\Sigma M_{nc} / \Sigma M_{nb} = 1.2$ and $R_e = 3$

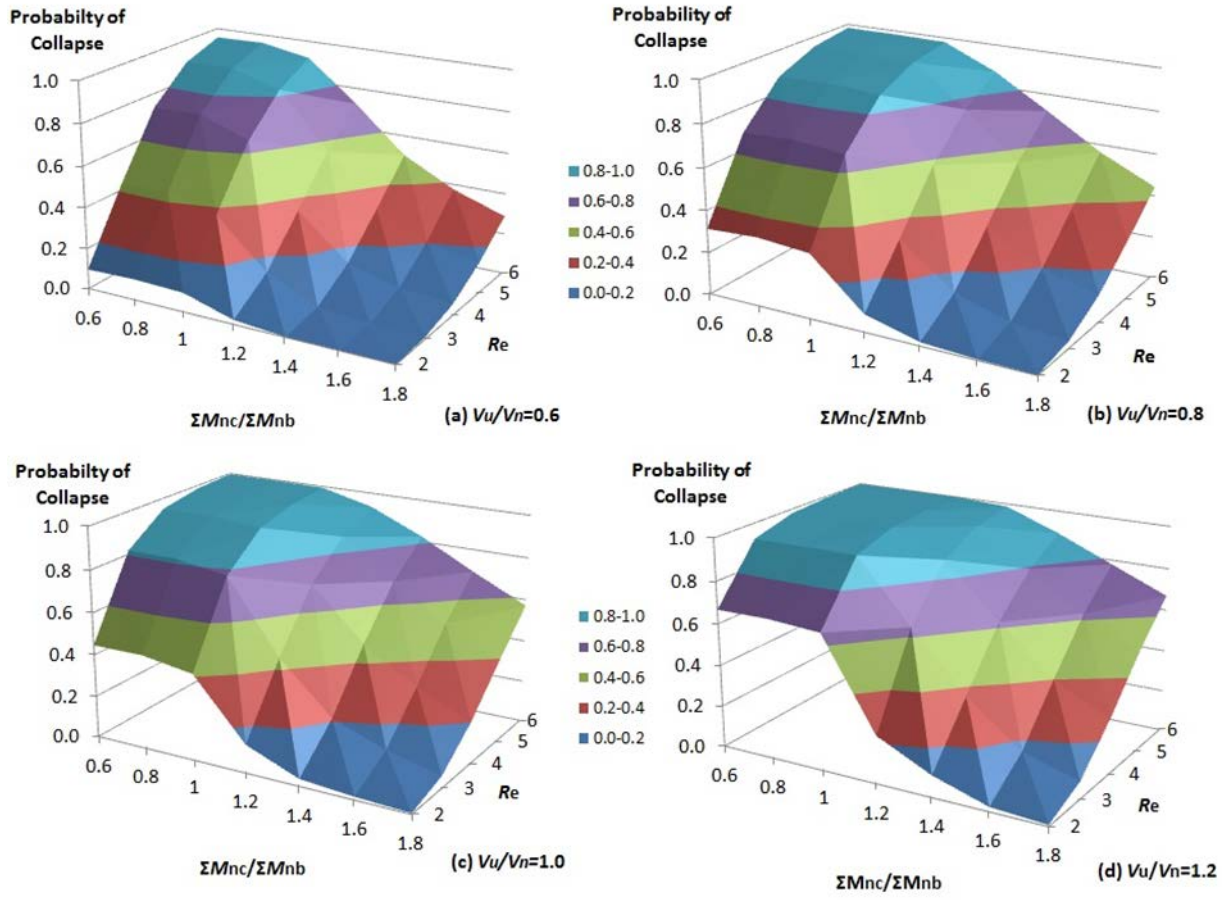

Figure 11. Comparison of the collapse performance of the 8-story bulding for (a) V_u/V_n=0.6 , (b) V_u/V_n=0.8, (c) V_u/V_n=1.0 and (d) V_u/V_n=1.2

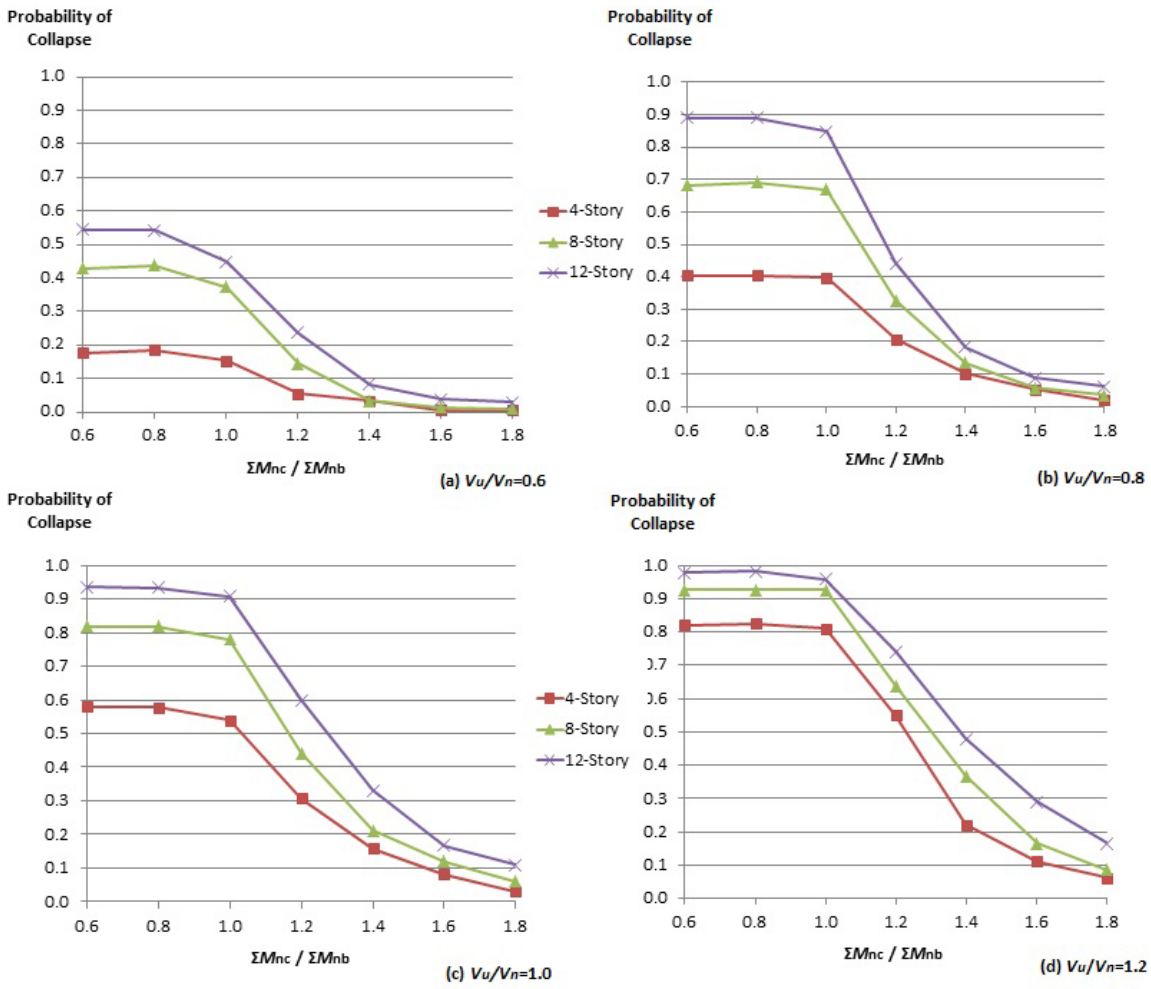

Figure 12. Comparison of the collapse performance of the three model buildings with R_e=3 for (a) V_u/V_n=0.6 , (b) V_u/V_n=0.8, (c) V_u/V_n=1.0 and (d) V_u/V_n=1.2

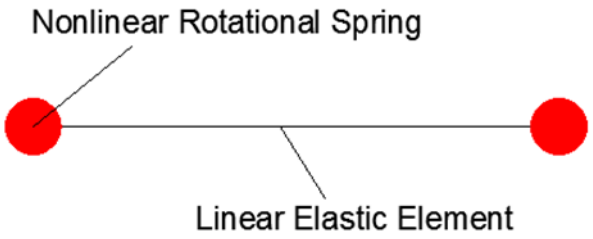

Figure A-1. Schematic illustration of the concentrated plasticity approach

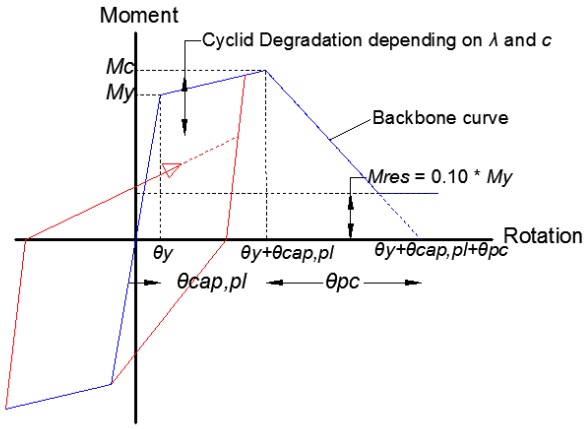

Figure A-2. Schematic plot of the backbone curve (blue line) and the cyclic curve (red line) of the spring-column element

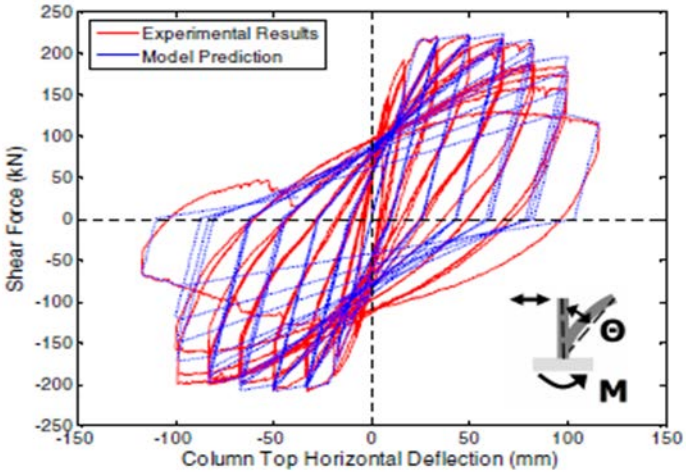

Figure A-3. Response of a calibrated spring-column element (Haselton et al., 2007)

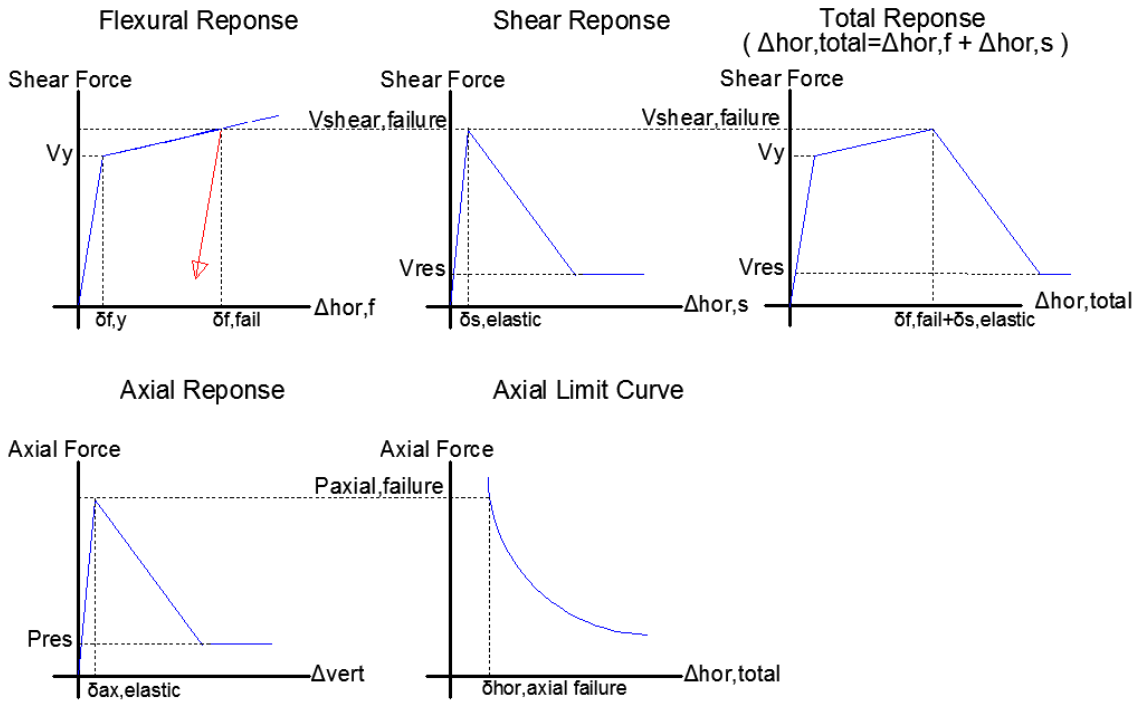

Figure A-4. Limit State Material (developed by Elwood and Moehle 2008)

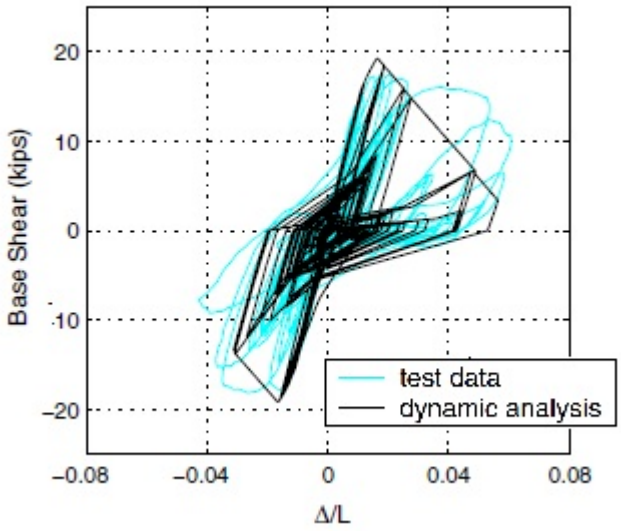

Figure A-5. Response of a calibrated Limit State Material (Elwood and Moehle 2003) where Δ corresponds to column top horizontal deflection and L to the column height

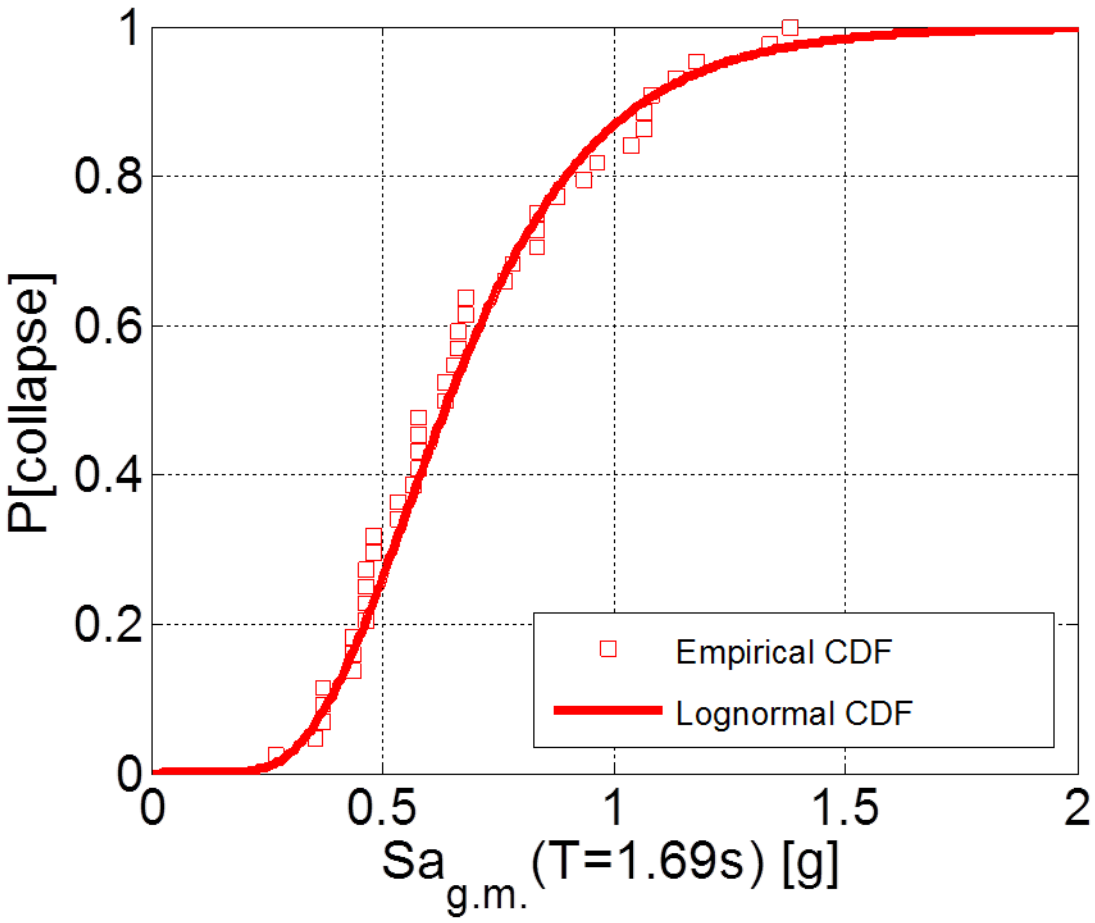

Figure B-1. Empirical and fitted Log-Normal Cumulative Distribution Function of Probability of Collapse (8-story building with $\Sigma M_{nc}/\Sigma M_{nb}$ = 1.2 and V_u/V_n=0.6).